

# FedMeld: A Model-dispersal Federated Learning Framework for Space-ground Integrated Networks

Qian Chen, *Member, IEEE*, Xianhao Chen, *Member, IEEE*, and Kaibin Huang, *Fellow, IEEE*

**Abstract**—To bridge the digital divide, the space-ground integrated networks (SGINs), which will be a key component of the six-generation (6G) mobile networks, are expected to deliver artificial intelligence (AI) services to every corner of the world. One mission of SGINs is to support federated learning (FL) at a global scale. However, existing space-ground integrated FL frameworks involve ground stations or costly inter-satellite links, entailing excessive training latency and communication costs. To overcome these limitations, we propose an infrastructure-free federated learning framework based on a model dispersal (FedMeld) strategy, which exploits periodic movement patterns and store-carry-forward capabilities of satellites to enable parameter mixing across large-scale geographical regions. We theoretically show that FedMeld leads to global model convergence and quantify the effects of round interval and mixing ratio between adjacent areas on its learning performance. Based on the theoretical results, we formulate a joint optimization problem to design the staleness control and mixing ratio (SC-MR) for minimizing the training loss. By decomposing the problem into sequential SC and MR subproblems without compromising the optimality, we derive the round interval solution in a closed form and the mixing ratio in a semi-closed form to achieve the *optimal* latency-accuracy tradeoff. Experiments using various datasets demonstrate that FedMeld achieves superior model accuracy while significantly reducing communication costs as compared with traditional FL schemes for SGINs.

**Index Terms**—Edge intelligence, federated learning, handover, space-ground integrated networks, convergence analysis.

## I. INTRODUCTION

Edge intelligence and space-ground integrated networks (SGINs) are two new features of sixth-generation (6G) mobile networks. Edge intelligence aims to deliver pervasive, real-time artificial intelligence (AI) services to users [1], [2], while SGINs ensure ubiquitous connectivity worldwide [3]. The convergence of these two trends in 6G marks a transformative step toward integrating networking and intelligence in space, enabling AI services to reach every corner of the planet. For instance, the Starlink constellation has deployed over 30,000 Linux nodes and more than 6,000 microcontrollers in space [4], creating a satellite server network orbiting around the Earth. This advancement extends traditional 2D edge AI into a 3D space-ground integrated AI paradigm [5], offering mission-critical AI services — such as healthcare, crop monitoring, and emergency response — anytime, anywhere [6]. One primary objective of space-ground integrated AI is to enable federated learning (FL) [5], referred to as space-ground

integrated FL (SGI-FL). Based on such technologies, pervasive ground clients collaboratively train AI models without sharing raw data [7], [8], while satellites act as parameter servers to periodically receive from, aggregate over, and redistribute model parameters to ground clients.

SGI-FL generally aims to train a global consensus model across a *large-scale geographical area* by learning from distributed data, i.e., training a healthcare AI model from hospitals and clinics across sparsely populated areas. Since a parameter server in SGI-FL, such as a low Earth orbit (LEO) satellite, can only cover a limited area [9], cooperation among multiple satellites is often needed. There are two primary approaches to synchronizing models among these satellite servers. The first approach is *mixing via ground stations*, where each satellite server transmits its aggregated model to a ground station for reaching global consensus. However, since a training round cannot finish until *all* satellites transmit their local updates to the ground station and receive the updated global model [10], [11], this approach often results in prolonged idle periods of up to several hours per round. To mitigate excessive waiting time, asynchronous FL can be employed, where aggregation is triggered as long as a preset number of models are received by the ground station [12]–[14]. Nevertheless, the mixing ratio between current and historical models during weighted averaging in these schemes has been demonstrated only empirically, leaving theoretical analysis unexplored. The other approach is *mixing via inter-satellite links* (ISLs), where satellites exchange the aggregated parameters with their neighboring satellites through ISLs. This approach can overcome the limited contact time between satellites and ground stations, accelerating the learning process through frequent model exchanges [15], [16]. However, it generates substantial data traffic within the satellite constellations. Furthermore, ISLs are not fully supported in many LEO mega-constellations due to the prohibitively high cost of laser terminals [17]. As a result, many LEO mega-constellations today still rely on bent-pipe frameworks, where data is routed via ground stations [18], [19]. In a nutshell, existing SGI-FL schemes, when serving large-scale regions through multiple satellites, face three major limitations: 1) dependence on ground stations, thereby leading to excessive waiting time, 2) reliance on ISLs, which may not be available, and 3) causing extra communication costs.

SGI-FL features high mobility of satellite servers. Outside the area of SGI-FL, some works have explored mobility-aware FL schemes in terrestrial networks [20]–[23]. Such works often adopt discrete Markov chains to model user mobility, using transition probabilities representing the likelihood of

Q. Chen, X. Chen, and K. Huang are with the Department of Electrical and Electronic Engineering, The University of Hong Kong, Hong Kong (Email: {qchen, xchen, huangk}@eee.hku.hk). Corresponding authors: X. Chen and K. Huang.

mobile users staying with or moving to neighboring edge servers. However, unlike terrestrial users with unpredictable movements, satellites move at high speeds along predetermined and repetitive orbital trajectories [24]. As a result, theoretical models like random walks or Markov chains, commonly used for terrestrial FL, are invalid for SGI-FL. Moreover, in terrestrial networks, parameter servers usually remain stationary. In contrast, in SGI-FL, parameter servers are moving, whereas ground clients are relatively static, as their speeds are negligible as compared with those of satellites [25]. Consequently, existing schemes for mobility-aware terrestrial FL networks cannot be applied to SGI-FL. Effectively supporting FL across large-scale geographical regions in the context of SGINs remains an open problem.

In this paper, to overcome all the above issues, we propose an SGI-FL framework called Federated learning with Model Dispersal (FedMeld) as our answer. FedMeld enables *infrastructure-free* model aggregation across large-scale geographical regions, eliminating the need for ground stations or ISLs. Our mechanism is inspired by a key observation: Given the repetitive trajectories and store-carry-forward (SCF) capabilities of co-orbital satellites, a satellite can transfer model parameters from one serving region  $i$  to the next region  $i + 1$  by mixing models from these two adjacent areas; Similarly, the circular nature of satellite orbits ensures that the model parameters from region  $i + 1$  will eventually be returned to region  $i$ . Consequently, without requiring dedicated ground stations or ISLs, *parameter mixing across all regions is naturally achieved through model dispersal via satellite trajectories*, akin to how animals disperse seeds across continents. In this way, FedMeld exploits the unique movement patterns of satellites, turning their high mobility from a foe to a friend. Within the FedMeld framework, users can continue training while satellites carrying model parameters traverse between adjacent regions, introducing a latency-accuracy tradeoff in managing model staleness. Moreover, model mixing ratios across regions should also be determined judiciously to achieve optimal learning performance. In this direction, we will answer two fundamental questions in FedMeld: 1) Does the proposed model dispersal method ensure global model convergence? and 2) how can we manage model staleness and mixing ratios to optimize training convergence? Our main contributions are summarized as follows:

- **FedMeld and Convergence Analysis:** We propose the FedMeld framework for efficient decentralized FL in SGINs. To support effective control, we theoretically characterize the convergence bound of FedMeld under both full and partial participation scenarios, accounting for the effects of model staleness and model mixing ratio. The results reveal a tradeoff between latency and accuracy. Specifically, increasing the global round interval of model mixing between adjacent regions accelerates the completion of the predefined training time but at the cost of reduced model accuracy. Furthermore, the model mixing ratio exhibits a strong coupling with the degree of model staleness, underscoring the necessity for optimal control strategies.

- **Control of Model Staleness and Mixing Ratio:** Building on the theoretical insights, we formulate a joint optimization problem to determine the staleness control and mixing ratio (SC-MR) that minimizes the training loss. This optimization problem is decomposed into two sequential subproblems without compromising optimality. We derive the optimal solutions for both decision variables in closed and semi-closed forms, respectively. The following design insights can be obtained from the theoretical solutions: Under more stringent training latency constraints, the round interval of model mixing becomes larger. Furthermore, when the non-IID degree of data is higher, the mixing ratio of historical models should be reduced.
- **Experimental Results:** We perform extensive simulations on diverse datasets to validate the effectiveness of our framework. Compared with existing solutions, FedMeld is not only infrastructure-free but also achieves higher accuracies with reduced training time.

The remainder of this paper is organized as follows. Models and metrics are introduced in Section II. The FedMeld algorithm and its convergence analysis are detailed in Section III. Building upon the convergence analysis, the joint optimization problem of SC-MR is formulated, and the optimal solutions are derived in Section IV. Experimental results are provided in Section V, followed by concluding remarks in Section VI.

## II. MODELS AND METRICS

As illustrated in Fig. 1, we consider an FL framework in SGINs, where a mega-LEO satellite constellation collaborates with groups of terrestrial edge devices to train a neural network model. The learning and communication models are described in separate subsections.

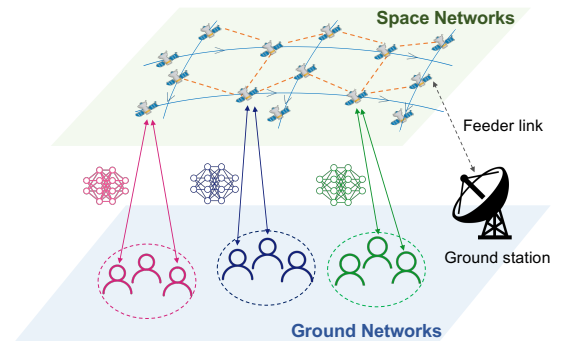


Fig. 1. An FL system in SGINs.

### A. Learning Model

The constellation consists of multiple circular orbits, with satellites uniformly distributed at equal distance intervals within each orbit. These AI-empowered satellites act as parameter servers and move along predetermined orbits. We assume that there are a set  $\mathcal{M}$  areas and a set of  $\mathcal{N}$  ground edge devices, with  $\mathcal{M} = \{1, \dots, M\}$  and  $\mathcal{N} = \{1, \dots, N\}$ . These ground areas are distributed along a specific orbit, and each

area  $i \in \mathcal{M}$  covers a subset of devices, denoted by  $\mathcal{N}_i$  with cardinality  $N_i$ .

The training process consists of  $R$  iterations (steps), denoted by  $\mathcal{R} = \{1, \dots, R\}$ . We assume that each serving satellite aggregates the model from its covered clients every  $E$  iterations, and we define  $\mathcal{I}_E = \{kE | k = 1, 2, \dots, \lfloor \frac{R}{E} \rfloor\}$  as the set of synchronization steps of each area, where  $k$  is the index of the global round. Since the devices in the same region are located nearby, we assume that they will be handed over to a new satellite parameter server at the same time according to some criteria such as distance and signal-to-noise ratio (SNR). In addition, considering partial device participation, in the  $k$ -th global round, the serving (nearest) satellite of area  $i$  randomly selects a device set,  $\mathcal{U}_{k,i}$  (with cardinality  $U_i$ ), out of  $\mathcal{N}_i$  to participate in the training process.

Let  $\mathbf{w}_{t,j}$  be the model parameters of device  $j$  at step  $t \in \mathcal{R}$ . When  $t \in \mathcal{I}_E$ , the models of devices in the same area will be aggregated by the serving satellite. Then, the update rule of device  $j$  can be given by

$$\mathbf{v}_{t+1,j} = \mathbf{w}_{t,j} - \eta_t \nabla F_j(\mathbf{w}_{t,j}, \zeta_{t,j}), \quad (1)$$

where  $\eta_t$  is the learning rate and  $\zeta_{t,j}$  is the selected batch from device  $j$  at step  $t$  with  $|\zeta|$  data samples. Here,  $\mathbf{v}_{t+1,j}$  is an auxiliary variable to denote the intermediate result of one step stochastic gradient descent (SGD) update from  $\mathbf{w}_{t,j}$ .

Motivated by [26], for the full participation scheme, we define two global virtual sequences as  $\bar{\mathbf{w}}_t = \frac{1}{M} \sum_{i \in \mathcal{M}} \bar{\mathbf{w}}_{t,i} = \frac{1}{M} \sum_{i \in \mathcal{M}} \frac{1}{N_i} \sum_{j \in \mathcal{N}_i} \mathbf{w}_{t,j}$  and  $\bar{\mathbf{v}}_t = \frac{1}{M} \sum_{i \in \mathcal{M}} \bar{\mathbf{v}}_{t,i} = \frac{1}{M} \sum_{i \in \mathcal{M}} \frac{1}{N_i} \sum_{j \in \mathcal{N}_i} \mathbf{v}_{t,j}$ , where  $\bar{\mathbf{w}}_{t,i}$  and  $\bar{\mathbf{v}}_{t,i}$  are area  $i$ 's virtual sequences. When  $t \notin \mathcal{I}_E$ , both global and area's sequences are inaccessible. When  $t \in \mathcal{I}_E$ , only  $\bar{\mathbf{w}}_{t,i}$  can be fetched for area  $i$ . After the last training step  $R$ , we assume that the models can be averaged over all areas to obtain the final global model  $\bar{\mathbf{w}}_R$ . For the general partial participation scheme, the global virtual sequence  $\bar{\mathbf{w}}_t$  is substituted by  $\bar{\mathbf{z}}_t = \frac{1}{M} \sum_{i \in \mathcal{M}} \frac{1}{U_i} \sum_{j \in \mathcal{U}_{t,i}} \mathbf{w}_{t,j}$ .

## B. Communication Model

The training process is conducted in consecutive global rounds until the stopping condition is reached. Since the total latency of each global round is limited, it is reasonable to assume that the network topology of SGINs remains unchanged during each global round. Without loss of generality, we focus on the global round  $k$  and one ground area  $i \in \mathcal{M}$  for analysis and provide detailed latency expressions as follows.

First, the selected clients conduct  $E$  local iterations, and the local computing latency of client  $j \in \mathcal{U}_{k,i}$  is calculated as

$$T_j^{\text{local}} = \frac{E|\zeta|\Phi}{L_j}, \quad \forall j \in \mathcal{N}, \quad (2)$$

where  $\Phi$  is the computing workload of local iteration and  $L_j$  denotes the computing capability (namely the number of floating point operations per second) of client  $j$ .

Then, clients in each area upload their models to their connected satellites. We consider orthogonal frequency-division multiple access (OFDMA) for uplink transmissions, and each

selected device per global round is assigned a dedicated sub-channel with bandwidth  $W^U$ . Then, the uplink rate between device  $j$  and its connected satellite at global round  $k$  can be expressed as

$$C_{k,j}^U = W^U \log_2 \left( 1 + \frac{P_{\text{UE}} G_{\text{UE}} G_{\text{SAT}} L_{k,j}^{\text{PL}} L^{\text{AL}}}{n_0 W^U} \right), \quad (3)$$

where  $P_{\text{UE}}$  is the transmit power of ground devices,  $G_{\text{UE}}$  and  $G_{\text{SAT}}$  are transmitting and receiving antenna gain of device and satellite, respectively. The free-space path loss  $L_{k,j}^{\text{PL}}$  is defined as  $L_{k,j}^{\text{PL}} = \left( \frac{\lambda_{k,j}}{4\pi d_{k,j}} \right)^2$ , where  $\lambda_{k,j}$  is the wavelength of uplink signal and  $d_{k,j}$  is the transmission distance. The additional loss  $L^{\text{AL}}$  is used to characterize the attenuation due to environmental factors, and  $n_0$  is the noise power spectral density. After the serving satellite conducts FedAvg with latency  $T_i^{\text{agg}}$ , the satellite broadcasts the averaged results to the clients, with the downlink rate between satellite and client  $j$  being

$$C_{k,j}^D = W^D \log_2 \left( 1 + \frac{P_{\text{SAT}} G_{\text{UE}} G_{\text{SAT}} L_{k,j}^{\text{PL}} L^{\text{AL}}}{n_0 W^D} \right), \quad (4)$$

where  $W^D$  is the bandwidth that the satellite broadcasts the global model to the users. In this paper, we focus solely on the applications for users in remote areas. Unlike urban environments with numerous blocks, remote regions have relatively few obstacles. Therefore, we disregard the impact of small-scale fading caused by the multi-path effect [27].

Given the data rate, the transmission latency over uplink and downlink can be expressed as  $T_{k,j}^U = \frac{q}{C_{k,j}^U}$  and  $T_{k,j}^D = \frac{q}{C_{k,j}^D}$ , where  $q$  denotes the number of bits within a model. Then, the total latency of global round  $k$  can be given by

$$T_{k,i}^{\text{total}} = \max_{j \in \mathcal{U}_{k,i}} \{ET_j^{\text{local}} + T_{k,j}^U + T_{k,j}^D\} + T_i^{\text{agg}}, \quad (5)$$

Since we consider the nearest association strategy, the serving duration of each satellite remains unchanged [28]. Thus, it can be regarded that during the period when a satellite provides connectivity to a specific region, the number of global training rounds it can participate in is fixed, denoted by  $K$ .

## C. Performance Metric

Each device  $j$  has a private dataset  $\mathcal{D}_j$  of size  $|\mathcal{D}_j|$ . Denote the  $n$ -th training data sample in device  $j$  by  $\xi_{j,n}$ , where  $n \in \mathcal{D}_j$ . The training objective of FL is to seek the optimal model parameter  $\mathbf{w}^*$  for the following optimization problem to minimize the global loss function:

$$\min_{\mathbf{w}} F(\mathbf{w}) = \frac{1}{M} \sum_{i \in \mathcal{M}} \frac{1}{N_i} \sum_{j \in \mathcal{N}_i} F_j(\mathbf{w}). \quad (6)$$

Here,  $F_j(\cdot)$  is the local objective, defined by

$$F_j(\mathbf{w}) \triangleq \frac{1}{|\mathcal{D}_j|} \sum_{n \in \mathcal{D}_j} \ell(\mathbf{w}, \xi_{j,n}), \quad (7)$$

where  $\ell(\cdot, \cdot)$  is a user-specified loss function.

At the  $t$ -th iteration, the convergence rate of FedMeld algorithm is defined as the expectation of the global loss

function at the  $t$ -th step, i.e.,  $F(\bar{\mathbf{w}}_t)$ , and the optimal objective value  $F(\mathbf{w}^*)$ , as

$$\mathbb{E}[F(\bar{\mathbf{w}}_t)] - F(\mathbf{w}^*). \quad (8)$$

### III. FEDMELD ALGORITHM AND CONVERGENCE ANALYSIS

In this section, we first describe our proposed FedMeld algorithm. Then, we conduct convergence analysis of FedMeld under full and partial participation schemes. The results are useful for optimizing the FedMeld in the next section.

#### A. FedMeld Algorithm

We divide the serving satellites into SCF satellites and non-SCF satellites. The former is the serving satellites which carry the latest models from regions until reaching the next serving area. The latter also acts as parameter servers, performs FedAvg for regions before the SCF satellites come, and does not store and carry models. For  $t \in \mathcal{I}_E$ , there are two cases:

1) When the serving satellite of area  $i$  is a non-SCF satellite, the devices within area  $i$  upload their models to this satellite for FedAvg.

2) When the serving satellite is an SCF satellite, area  $(i-1)$ 's model carried by this satellite can be mixed with area  $i$ 's model after performing FedAvg for the collected clients' model in step  $t$ .

Without loss of generality, we assume the handover occurs only at synchronization steps. To accelerate the training process, devices in each region continue additional training rounds with non-SCF satellites before the arrival of the incoming SCF satellite. We define the global round interval of model mixing between adjacent regions as  $\delta$ . During the stage from when the SCF satellite leaves the visible range of area  $i$  until the completion of model aggregation for area  $(i+1)$ , we define two parameters:  $T_{i,i+1}^{\text{fly}}$  and  $T_{i,i+1}^{\text{idle}}$ . Here,  $T_{i,i+1}^{\text{fly}}$  is the total duration of this process, and  $T_{i,i+1}^{\text{idle}}$  is the idle duration of clients in the region  $(i+1)$ , i.e., they are neither training with SCF satellites nor non-SCF satellites. Then, we have  $T_{i,i+1}^{\text{idle}} + \sum_{k'=k+1}^{k+\delta} T_{k',i+1}^{\text{total}} = T_{i,i+1}^{\text{fly}}$  for any  $k - K \bmod (K + \delta) = 0$ . Since we consider that all the regions are covered by a specific circular orbit, area  $i = 0$  is equivalent to the last area (i.e.,  $i = M$ ), and  $i = M + 1$  equals the first area (i.e.,  $i = 1$ ).

Let a binary variable,  $A_t \in \{0, 1\}$ , denote whether the area's model mixes with its adjacent model at step  $t$ , which is predetermined by the network topology of SGINs. Let  $\alpha$  denote the model mixing ratio of adjacent areas. Then, the model of device  $j \in \mathcal{N}_i$  at step  $t$  can be expressed as

$$\mathbf{w}_{t,j} = \begin{cases} \mathbf{v}_{t,j}, & \text{if } t \notin \mathcal{I}_E, \\ (1 - \alpha A_t) \bar{\mathbf{v}}_{t,i} + \alpha A_t \bar{\mathbf{w}}_{t-\delta E, i-1}, & \text{if } t \in \mathcal{I}_E. \end{cases} \quad (9)$$

Fig. 2 provides an example of how models from four regions are mixed. Here, red, blue, yellow, and green stars are SCF satellites that carry the latest models from four areas, i.e., A, B, C, and D, respectively, and will perform model mixing upon reaching the next serving area. Gray satellites are non-SCF satellites and can also act as parameter servers when an area is not covered by an SCF satellite. Their participation

leads to model staleness when mixing. Algorithm 1 shows the procedure of FedMeld, and the details are as follows.

- 1) At the beginning of a mix cycle, users in each area and their serving (nearest) SCF satellite execute  $K$  global rounds cooperatively until the handover happens. Specifically, when a global round starts, the SCF satellite selects a set of participating clients to conduct  $E$  local iterations. Then, the satellite collects the uploaded models from these users, runs FedAvg, and broadcasts the averaged model back to users.
- 2) Before the SCF satellite which carries area  $(i-1)$ 's model becomes the serving satellite for area  $i$ , users in region  $i$  and their connected non-SCF satellites conduct  $\delta - 1$  global rounds collaboratively.
- 3) When the SCF satellite serves for area  $i$ , users in region  $i$  conduct  $E$  local iterations and upload their models to this satellite. After running FedAvg for the collected models of area  $i$ , the satellite mixes this averaged result with its stored historical model of area  $(i-1)$ , where the mixing proportion of the historical model is  $\alpha$ .
- 4) Go back to Step 1) until the stopping condition is met.

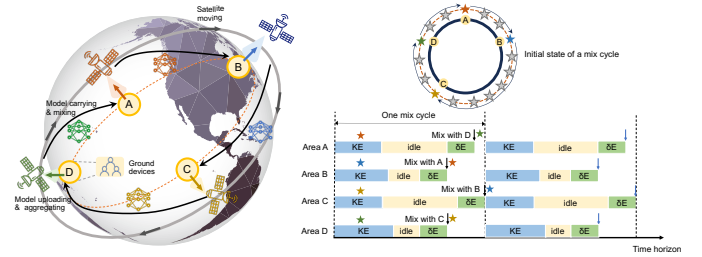


Fig. 2. An example diagram of parameter mixing in FedMeld algorithm.

In the FedMeld algorithm, each time an SCF satellite arrives at the next region, a parameter mixing occurs with adjacent regional models. Since these regions are covered by satellites on the same orbital plane, only  $M - 1$  mixing times are required for each region to incorporate parameter information from other regions, naturally achieving global model fusion with FedMeld.

#### B. Assumptions and Definitions

We proceed by making the widely adopted assumptions on client  $j$ 's local loss function  $F_j(\mathbf{w})$ . Let  $\nabla F_j(\mathbf{w}) \triangleq \mathbb{E}_{\zeta_j}[\nabla F_j(\mathbf{w}; \zeta_j)]$ .

**Assumption 1. ( $L$ -smoothness):** For device  $j \in \mathcal{N}$ ,  $F_j(\mathbf{w})$  is differentiable and there exists a constant  $L \geq 0$  such that for all  $\mathbf{w}$  and  $\mathbf{w}'$ ,  $F_j(\mathbf{w}) \leq F_j(\mathbf{w}') + (\mathbf{w} - \mathbf{w}')^T \nabla F_j(\mathbf{w}') + \frac{L}{2} \|\mathbf{w} - \mathbf{w}'\|^2$  holds.

**Assumption 2. ( $\mu$ -strongly convex):** For device  $j \in \mathcal{N}$ ,  $F_j(\mathbf{w}) \geq F_j(\mathbf{w}') + (\mathbf{w} - \mathbf{w}')^T \nabla F_j(\mathbf{w}') + \frac{\mu}{2} \|\mathbf{w} - \mathbf{w}'\|^2$  holds.

**Assumption 3. (Unbiasedness and bounded stochastic gradient variance):** For device  $j \in \mathcal{N}$ , the stochastic gradient is unbiased with variance bounded by

---

**Algorithm 1** FedMeld Algorithm
 

---

1: **Input:** Learning rate  $\eta_t$ , number of local iterations  $E$ , number of total iterations  $R$ , handover condition  $A_t$ , number of global rounds trained by each SCF satellite  $K$ , mixing ratio  $\alpha$ , global round interval of model mixing between adjacent regions  $\delta$

2: **Output:** Model parameter  $\mathbf{w}$

3: Initialize model parameter  $\mathbf{w}$  with  $\mathbf{w}_0$

4: **for** each global round  $k = 1, 2, \dots, \frac{R}{E}$  **do**

5:   **for** each serving satellite of area  $i = 1 \dots M$  **parallel do**

6:     Randomly select a set of active clients  $\mathcal{U}_{k,i}$

7:     **for** each client  $j \in \mathcal{U}_{k,i}$  in parallel **do**

8:       **if**  $t \notin \mathcal{I}_E$  **then**

9:          $\mathbf{w}_{t,j} = \mathbf{v}_{t,j}$

10:       **else**

11:          $\mathbf{w}_{t,j} = (1 - \alpha A_t) \bar{\mathbf{v}}_{t,i} + \alpha A_t \bar{\mathbf{w}}_{t-\delta E, i-1}$

12:       **end if**

13:     **end for**

14:   **end for**

15: **end for**

16: **return**  $\mathbf{w}$

---

$\sigma^2$  such that  $\mathbb{E}[\nabla F_j(\mathbf{w}_j; \varsigma_j)] = \nabla F_j(\mathbf{w}_j)$  and  $\mathbb{E}_{\varsigma_j} \|\nabla F_j(\mathbf{w}_j; \varsigma_j) - \nabla F_j(\mathbf{w}_j)\|^2 \leq \sigma_j^2$  for all  $\mathbf{w}$ .

**Assumption 4.** (Bounded gradient): The expected value of the squared norm of stochastic gradients is consistently bounded:  $\|\nabla F_j(\mathbf{w}_j; \varsigma_j)\|^2 \leq G^2$  for all  $j \in \mathcal{N}$ .

We also quantify the degree of non-independent and identically distributed (non-IID) based on the following definition.

**Definition 1.** (Degree of non-IID) Let  $F^*$  and  $F_j^*$  be the minimum values of  $F$  and  $F_j$ , respectively. We use a constant  $\Gamma$ , denoted by  $\Gamma = F^* - \frac{1}{M} \sum_{i \in \mathcal{M}} \frac{1}{N_i} \sum_{j \in \mathcal{N}_i} F_j^*$ , to quantify the non-IID degree of data in SGINs.

If the data are IID,  $\Gamma$  goes to zero when the number of data increases. If the data are non-iid, we will have  $\Gamma > 0$  and its magnitude shows the data heterogeneity.

### C. Convergence Analysis

We first analyze the convergence bound of FedMeld under the full participation scheme and then extend the result to the partial participation one.

**Lemma 1.** (Results of one step SGD [26, Lemma 1]) Let assumption 1 and 2 hold. Notice that  $\bar{\mathbf{v}}_{t+1} = \bar{\mathbf{w}}_t - \eta_t \mathbf{g}_t$  always holds. If  $\eta_t \leq \frac{1}{4L}$ , we have

$$\begin{aligned} \|\bar{\mathbf{v}}_{t+1} - \mathbf{w}^*\|^2 &\leq (1 - \mu \eta_t) \mathbb{E} \|\bar{\mathbf{w}}_t - \mathbf{w}^*\|^2 + \eta_t^2 \mathbb{E} \|\mathbf{g}_t - \bar{\mathbf{g}}_t\|^2 \\ &+ 6L\eta_t^2 \Gamma + 2\mathbb{E} \sum_{i \in \mathcal{M}} \sum_{j \in \mathcal{N}_i} \frac{1}{MN_i} \|\mathbf{w}_{t,j} - \bar{\mathbf{w}}_t\|^2, \end{aligned} \quad (10)$$

where  $\mathbf{g}_t = \frac{1}{M} \sum_{i \in \mathcal{M}} \frac{1}{N_i} \sum_{j \in \mathcal{N}_i} \nabla F_j(\mathbf{w}_{t,j}, \varsigma_{t,j})$ ,  $\bar{\mathbf{g}}_t = \frac{1}{M} \sum_{i \in \mathcal{M}} \frac{1}{N_i} \sum_{j \in \mathcal{N}_i} \nabla F_j(\mathbf{w}_{t,j})$ , and  $\Gamma = F^* - \sum_{i \in \mathcal{M}} \sum_{j \in \mathcal{N}_i} \frac{1}{MN_i} F_j^*$ .

Define function  $m(\alpha) = \frac{4(1-\alpha)(2\alpha^2-\alpha+1)}{\alpha(2\alpha^2-3\alpha+3)}$ . With Lemma 1, we have the following theorem to provide the convergence bound of FedMeld under full participation scheme.

**Theorem 1.** (Convergence bound under full participation scheme) Choose the learning rate  $\eta_t = \frac{5}{\mu(\gamma+t)}$  for  $\gamma = \max\left\{\frac{8L}{\mu}, E\right\} - 1$ , when  $\delta E \leq \frac{m(\alpha)(t+\gamma+1)^2}{(t+\gamma)^2+m(\alpha)(t+\gamma+1)}$ , the convergence bound with full participation at the last time step  $R$  satisfies

$$\begin{aligned} \mathbb{E}[F(\bar{\mathbf{w}}_R)] - F(\mathbf{w}^*) &\leq \left(\frac{1}{1-\alpha} - \alpha + \frac{1}{2}\right) \frac{L}{\mu(R+\gamma)} \\ &\cdot \left[\frac{25B}{8\mu} + \frac{\mu(\gamma+1)}{2} \mathbb{E} \|\bar{\mathbf{w}}_1 - \mathbf{w}^*\|^2\right] + LQ_{R-1}, \end{aligned} \quad (11)$$

where  $Q_{R-1} = \mathbb{E} \sum_{i \in \mathcal{M}} \sum_{j \in \mathcal{N}_i} \frac{1}{MN_i} \|\mathbf{w}_{R-1,j} - \bar{\mathbf{w}}_{R-1}\|^2$  and  $B = \sum_{i \in \mathcal{M}} \sum_{j \in \mathcal{N}_i} \frac{\sigma_j^2}{(MN_i)^2} + 6L\Gamma$ .

*Proof.* Please see Appendix A.  $\square$

**Lemma 2.** For any  $t \geq 0$  satisfying  $t \in \mathcal{I}_E$ ,  $Q_t = \mathbb{E} \sum_{i \in \mathcal{M}} \sum_{j \in \mathcal{N}_i} \frac{1}{MN_i} \|\mathbf{w}_{t,j} - \bar{\mathbf{w}}_t\|^2$  has the following upper bound,

$$\begin{aligned} Q_t &\leq (1+b)(1-\alpha A_t)^2 Q_{t-E} + (1+b)(\alpha A_t)^2 Q_{t-\delta E} \\ &+ 4 \left(1 + \frac{1}{b}\right) (1-\alpha A_t)^2 (E-1)^2 G^2 \eta_t^2, \end{aligned} \quad (12)$$

For  $t \notin \mathcal{I}_E$ , we can always find a  $\tilde{t}$  such that  $\tilde{t} = \lfloor \frac{t}{E} \rfloor E$ . Then,  $Q_t$  has the following upper bound,

$$Q_t \leq (1+b) Q_{\tilde{t}} + 4 \left(1 + \frac{1}{b}\right) (E-1)^2 G^2 \eta_t^2. \quad (13)$$

Here,  $b$  is a positive constant, and its value will be discussed in detail in the subsequent paragraphs.

*Proof.* Please see Appendix B.  $\square$

Based on Lemma 2, the term  $Q_{R-1}$  can be upper bounded as follows.

**Theorem 2.** Assume that  $R-1$  is the final step of a particular mix cycle. The upper bound of  $Q_{R-1}$  satisfies

$$Q_{R-1} \leq \eta_E^2 \frac{\kappa_2}{1-\kappa_1}, \quad (14)$$

where  $\kappa_1 = (1+b)^{K+\delta} (1-\alpha)^2 + (1+b)\alpha^2$  and  $\kappa_2 = 4 \left(1 + \frac{1}{b}\right) (E-1)^2 G^2 \left[\frac{\kappa_1}{b} + (1-\alpha)^2\right]$ . Here,  $\kappa_1 < 1$ .

*Proof.* Please see Appendix C.  $\square$

After completing the analysis of the full participation scheme, we extend this result to the partial participation scenario as follows.

**Lemma 3.** (Bounding average variance under unbiased sampling scheme [29, Lemma 1]) If  $t$  is a global round and satellites select clients randomly without replacement, then

$\mathbb{E}_{\mathcal{U}_t} \bar{\mathbf{z}}_t = \bar{\mathbf{w}}_t$ , where  $\mathcal{U}_t = \bigcup_{i \in \mathcal{M}} \mathcal{U}_{t,i}$  represents the union of selected clients. Due to partial participation, we have

$$\mathbb{E}_{\mathcal{U}_t} \|\bar{\mathbf{z}}_t - \bar{\mathbf{w}}_t\|^2 \leq \frac{1}{M^2} \sum_{i \in \mathcal{M}} \frac{N_i - U_i}{U_i N_i (N_i - 1)} \sum_{j \in \mathcal{N}_i} \|\mathbf{w}_{t,j} - \bar{\mathbf{w}}_t\|^2. \quad (15)$$

For notational brevity, we denote constants  $\zeta_1, \zeta_2, \zeta_3$  as follows,

$$\begin{cases} \zeta_1 = \frac{L}{\mu(R+\gamma)} \left[ \frac{25B}{8\mu} + \frac{\mu(\gamma+1)}{2} \mathbb{E} \|\bar{\mathbf{w}}_1 - \mathbf{w}^*\|^2 \right], \\ \zeta_2 = L \left[ \frac{1+b}{2} \max_{i \in \mathcal{M}} \left\{ \frac{N_i - U_i}{MU_i(N_i - 1)} \right\} + 1 \right], \\ \zeta_3 = 2L \left( 1 + \frac{1}{b} \right) (E - 1)^2 G^2 \eta_R^2 \max_{i \in \mathcal{M}} \left\{ \frac{N_i - U_i}{MU_i(N_i - 1)} \right\}. \end{cases}$$

Based on Lemma 3, the convergence bound under the partial participation scheme is provided in the following theorem.

**Theorem 3.** (Convergence Bound under Partial Participation) *With an unbiased sampling scheme, the convergence bound with partial client participation at step  $R$  can be expressed as*

$$\mathbb{E} [F(\bar{\mathbf{z}}_R)] - F(\mathbf{w}^*) \leq \zeta_1 \left( \frac{1}{1-\alpha} - \alpha + \frac{1}{2} \right) + \zeta_2 \frac{\kappa_2}{1-\kappa_1} + \zeta_3. \quad (16)$$

*Proof.* Please see Appendix D.  $\square$

**Remark 1.** (Impact of partial participation): *The partial participation scheme will bring an additional term reflected by  $\max_{i \in \mathcal{M}} \frac{N_i - U_i}{MU_i(N_i - 1)}$ . When  $U_i$  is larger, the negative effect caused by this term will be mitigated. In the extreme case that all clients join the training process, this term will be eliminated.*

**Remark 2.** (Discussion of  $b$  in Theorem 2): *It is clear that  $\kappa_1$  has the following upper bound, i.e.,  $\kappa_1 \leq (1+b)^{K+\delta} c^2 \cdot \max \left\{ \alpha^2, (1-\alpha)^2 \right\}$ , where  $c \geq 1$ . Define an auxiliary variable  $\rho$  satisfying  $1 < \rho \leq \min \left\{ \frac{1}{\alpha}, \frac{1}{1-\alpha} \right\}$ . When choosing  $b = \rho^{\frac{1}{K+1}} - 1$  and  $c = \frac{1}{\rho \cdot \max \left\{ \alpha, 1-\alpha \right\}} \geq 1$  for  $\delta < K + 2$ ,  $\kappa_1 < 1$  can be guaranteed. Then,  $\kappa_1$  and  $\kappa_2$  can be recast as*

$$\begin{cases} \kappa_1 = \rho^{\frac{K+\delta}{K+1}} (1-\alpha)^2 + \rho \alpha^2, \\ \kappa_2 = 4(E-1)^2 G^2 \frac{\rho^{\frac{1}{K+1}}}{\rho^{\frac{1}{K+1}} - 1} \left[ \frac{\rho^{\frac{K+\delta}{K+1}} (1-\alpha)^2 + \rho \alpha^2}{\rho^{\frac{1}{K+1}} - 1} + (1-\alpha)^2 \right]. \end{cases} \quad (17)$$

For simplicity,  $\rho$  can be set as  $\frac{3}{2}$ .

**Remark 3.** (Impact of  $\delta$  and  $\alpha$  on model accuracy): *Given the communication scenario and initial training setting in SGINs,  $E$ ,  $G$ , and  $K$  (since the training rounds of each serving satellite are stable in the long term) are fixed. Therefore, the model loss in (16) can be adjusted by designing parameters  $\delta$  and  $\alpha$ . We can find that the right side of (16) is a monotonically increasing function of  $\delta$ , indicating the tradeoff between latency and accuracy. However, the coupling relationship between  $\delta$  and  $\alpha$  not only exists in the upper bound of model loss but also in the constraint presented in (1). Their complex dependency makes it challenging to derive their joint optimal solutions, motivating us to formulate an optimization problem and design an algorithm in the next section.*

## IV. FEDMELD OPTIMIZATION

In this section, the results from the preceding convergence analysis are applied to the FedMeld optimization. First, we formulate a joint optimization problem of SC-MR to minimize the model loss under FedMeld within a fixed span of training time. Then, we demonstrate that the problem can be decomposed into two consecutive subproblems, which can be optimally solved using the algorithm we proposed.

### A. Problem Formulation

To ensure convergence performance, we formulate an optimization problem to find the optimal global round interval of model mixing  $\delta$  and model mixing ratio  $\alpha$ , which is cast as follows:

$$\mathcal{P}1 : \min_{\delta, \alpha} f(\delta, \alpha) = \zeta_1 \left( \frac{1}{1-\alpha} - \alpha + \frac{1}{2} \right) + \zeta_2 \frac{\kappa_2}{1-\kappa_1} + \zeta_3 \quad (18a)$$

$$\text{s.t. } T_{i,i+1}^{\text{idle}} + \sum_{k'=k+1}^{k+\delta} T_{k',i+1}^{\text{total}} = T_{i,i+1}^{\text{fly}}, \quad (18b)$$

$$\forall k : k - K \bmod (K + \delta) = 0, i \in \mathcal{M},$$

$$\frac{R-1}{(K+\delta)E} \cdot \max_{i \in \mathcal{M}} \left\{ T_{i,i+1}^{\text{fly}} \right\} \leq T_{\max}, \quad (18c)$$

$$\delta E \leq \frac{m(\alpha)(t+\gamma+1)^2}{(t+\gamma)^2 + m(\alpha)(t+\gamma+1)}, \quad \forall t \in \mathcal{R}, \quad (18d)$$

where the objective (18a) is to optimize the convergence bound. Constraint (18b) ensures that the sum of idle duration and additional training time equals the satellite flight time between two adjacent areas. Constraint (18c) ensures that the total training time does not exceed the maximum constraint. Constraint (18d) limits the maximal round gap of the mixed models, which has been discussed in detail earlier in Theorem 1.

### B. Equivalent Problem Decomposition

The joint SC-MR problem can be decoupled into two sequential subproblems. The first subproblem SC is to minimize the model staleness with relevant constraints from  $\mathcal{P}1$ , which can be expressed as

$$(\mathcal{P}2 : \text{SC}) \quad \min \delta$$

$$\text{s.t. (18b) \& (18c).}$$

Given the optimal model staleness indicator  $\delta^*$  from solving  $\mathcal{P}2$ , the second subproblem MR can be simplified from  $\mathcal{P}1$  as

$$(\mathcal{P}3 : \text{MR}) \quad \min_{\alpha} f(\delta^*, \alpha)$$

$$\text{s.t. } \delta^* E \leq \frac{m(\alpha)(t+\gamma+1)^2}{(t+\gamma)^2 + m(\alpha)(t+\gamma+1)}, \quad \forall t \in \mathcal{R}.$$

The optimality of the aforementioned decomposition is demonstrated in the following lemma.

**Lemma 4.** *Solving  $\mathcal{P}1$  is equivalent to first solving  $\mathcal{P}2$  and then solving  $\mathcal{P}3$ .*

*Proof.* The feasibility of  $\mathcal{P}1$  indicates the right side of (18d) is large enough. It is clear that the objective function  $f(\delta, \alpha)$  of  $\mathcal{P}1$  is monotonically increasing with respect to  $\delta$ . Simultaneously, the right side of (18d) is a monotonically decreasing function with respect to  $\alpha$ . Thus, solving  $\mathcal{P}2$ , which can obtain the minimal value of  $\delta$  (i.e.,  $\delta^*$ ), can allow for a larger range of values for  $\alpha$ . It can increase the likelihood of  $\alpha$  reaching its optimal solution. Conditioned on  $\delta^*$ , the optimal mixing ratio policy is simplified to  $\mathcal{P}3$ .  $\square$

### C. Optimal Solutions of Joint SC-MC Design

1) *Optimal Solution of  $\delta$ :* Since only Constraint (18c) limits the lower bound of  $\delta$ , the optimal  $\delta$  denoted by  $\delta^*$  is given by

$$\delta \geq \delta^* = \frac{R-1}{ET_{\max}} \cdot \max_i \left\{ T_{i,i+1}^{\text{fly}} \right\} - K. \quad (21)$$

2) *Optimal Solution of  $\alpha$ :* First, we discuss the feasible set of  $\alpha$ . By taking the derivative, we can find that if the monotonic decreasing function  $m(\alpha)$  satisfies  $m(\alpha) \geq 2$ , i.e.,  $\alpha \leq \frac{1}{2}$ , the right side of (18d) is a non-decreasing function of  $t$ . Therefore, as long as  $\delta^*E \leq \frac{m(\alpha)[(K+\delta^*)E+\gamma]^2}{[(K+\delta^*)E+\gamma-1]^2+m(\alpha)[(K+\delta^*)E+\gamma]}$  holds, which is equivalent to

$$m(\alpha) \geq \frac{\delta^*E[(K+\delta^*)E+\gamma-1]^2}{[(K+\delta^*)E+\gamma](KE+\gamma)}, \quad (22)$$

then (18d) can be always satisfied. Let  $\tilde{\alpha}$  be the value of  $\alpha$  which makes (22) an equality. Thus, the feasible set of  $\alpha$  is  $\alpha \in [0, \min\{\tilde{\alpha}, \frac{1}{2}\}]$ .

Then, we analyze the derivative of  $f(\delta^*, \alpha)$  and obtain the optimal solution of  $\alpha$ . By taking the derivative, we have

$$f'(\alpha) = \frac{\partial f(\delta^*, \alpha)}{\partial \alpha} = \zeta_1 \left[ \frac{1}{(1-\alpha)^2} - 1 \right] + \zeta_2 \frac{g_1(\alpha)}{[g_2(\alpha)]^2}, \quad (23)$$

where  $g_1(\alpha) = \left[ \left( \rho^{\frac{K+\delta}{K+1}} + \rho \right) D_1 + (\rho+1) D_2 \right] \alpha - \left( \rho^{\frac{K+\delta}{K+1}} D_1 + D_2 \right)$  and  $g_2(\alpha) = \left( \rho^{\frac{K+\delta}{K+1}} + \rho \right) \alpha^2 - 2\rho^{\frac{K+\delta}{K+1}} \alpha + \rho^{\frac{K+\delta}{K+1}} - 1$ .

Here, we use  $D_1 = 4(E-1)^2 G^2 \frac{\rho^{\frac{1}{K+1}}}{\left( \rho^{\frac{1}{K+1}} - 1 \right)^2}$  and

$D_2 = 4(E-1)^2 G^2 \frac{\rho^{\frac{1}{K+1}}}{\rho^{\frac{1}{K+1}} - 1}$  for notation simplicity. Note that

$g_1(\alpha)$  is monotonically increasing when  $\alpha$  is no more than  $\frac{\left( \rho^{\frac{K+\delta}{K+1}} + \rho \right) D_1 + (\rho+1) D_2}{2\rho D_2}$ , which is less than  $\frac{1}{2}$ . Specifically,

$g_1(0) < 0$ ,  $g_1(\frac{1}{2}) < 0$  and  $g_1(1) > 0$  always hold. For  $g_2(\alpha)$ , its discriminant is negative, denoting that  $g_2(\alpha)$  is always positive. In addition,  $g_2(\alpha)$  is monotonically decreasing when  $\alpha \leq \frac{\rho^{\frac{K+\delta}{K+1}}}{\rho^{\frac{K+\delta}{K+1}} + \rho}$ , where  $\frac{\rho^{\frac{K+\delta}{K+1}}}{\rho^{\frac{K+\delta}{K+1}} + \rho}$  falls in the

range of  $[\frac{1}{2}, 1)$ . The characteristics of  $g_1(\alpha)$  and  $g_2(\alpha)$  show that  $\frac{g_1(\alpha)}{[g_2(\alpha)]^2}$  is monotonically increasing when  $\alpha \in [0, \frac{1}{2}]$ .

Simultaneously,  $\frac{1}{(1-\alpha)^2} - 1$  is a monotonically increasing function of  $\alpha$ . Thus, we can say that derivative function  $f'(\alpha)$  is non-decreasing with respect to  $\alpha \leq \frac{1}{2}$ . Combining with the constraint (22), the optimal solution  $\alpha^*$  can be determined by

$$\alpha^* = \min\{\hat{\alpha}, \tilde{\alpha}\}, \quad (24)$$

where

$$\hat{\alpha} = \begin{cases} \alpha_0 : f'(\alpha_0) = 0, & \text{if } f'(\frac{1}{2}) > 0, \\ \frac{1}{2}, & \text{if } f'(\frac{1}{2}) < 0. \end{cases} \quad (25)$$

Here,  $\alpha_0$  can be obtained by bisection method since the  $f'(\alpha)$  is monotonic and thus there is only one zero root if  $f'(\frac{1}{2}) > 0$ .

**Remark 4.** From (21), we have the following observation. When the training latency requirements become more stringent, or the satellite distribution becomes denser,  $\delta^*$  increases. This indicates that the difference in the global round interval of model mixing between adjacent regions becomes larger.

**Remark 5.** The large non-IID degree of data  $\Gamma$  leads to bigger  $\zeta_1$ . When  $\zeta_1$  is large enough,  $\alpha_0$  will be smaller, making  $\alpha^* < \frac{1}{2}$  possible. This implies that when the non-IID degree of data is larger, the mixing ratio of historical models from adjacent areas should be less.

## V. EXPERIMENTAL RESULTS

In this section, we conduct experiments to evaluate the proposed FedMeld in terms of model accuracy and time consumption in comparison with other baselines.

### A. Experiment Settings

In the simulations, we examine the SGINs consisting of an LEO constellation and  $N = 40$  ground devices. The constellation follows the Starlink system, consisting of 24 orbital planes with 66 satellites in each orbit, while the ground devices are distributed across  $M = 8$  clusters.

We conduct image classification tasks using the CIFAR-10 [30] and MNIST [31] datasets, employing the ResNet-18 architecture [32]. The CIFAR-10 dataset comprises 50,000 training samples and 10,000 testing samples across 10 categories, while MNIST contains 60,000 training samples and 10,000 testing samples with labels ranging from 0 to 9. Each client possesses an equal number of images, with distinct images allocated to each device. The computational capacity of each client is  $h_j = 15.11$  TFLOPS. In each global round, 80% of clients from each cluster are randomly selected to participate in the training process. Furthermore, we set  $E = 5$  [21] and  $|\zeta| = 64$  [33]. The initial learning rate is determined using a grid search method [29]. The maximum tolerable delay,  $T_{\max}$ , is 32 hours for CIFAR-10 and 20 hours for MNIST. Additional key wireless parameters are provided in Table I [34].

TABLE I  
MAIN PARAMETER SETTING

Parameter	Value
Uplink and downlink frequency, $\lambda_{k,j}$ and $\lambda_{k,j}$	14 GHz, 12 GHz
Transmit power, $P_{\text{UE}}$ and $P_{\text{SAT}}$	1 W and 5 W
Additional loss, $L^{\text{AL}}$	5 dB
Noise power spectral density $n_0$	$1.38 \times 10^{-21}$
Radius of satellite antenna	0.48 m
Radius of ground terminal antenna	0.5 m
Bandwidth of each active client	5 MHz

TABLE II  
COMPARISON OF TYPICAL FEDERATED LEARNING FRAMEWORK WITH  $M$  CLUSTERS AND  $U$  PARTICIPATING CLIENTS IN ONE GLOBAL ROUND

Learning Framework	HFL [10]	PFL [29]	Ring Allreduce [16]	Ours
Learning type	Centralized FL	Decentralized FL		
Model aggregation/exchanging method	Ground station	ISL		
Communication traffic (bits)	$2(U + M)q$	$2(U + 2M)q$	$2[U + (M - 1)]q$	$2Uq$
Number of established links	$2(Ul_{U2S} + Ml_{S2G})$	$\min : 2(Ul_{U2S} + 2Ml_{ISL})$ $\max : 2(Ul_{U2S} + 4Ml_{S2G})$	$\min :$ $2[Ul_{U2S} + M(M - 1)l_{ISL}]$ $\max :$ $2[Ul_{U2S} + 2M(M - 1)l_{S2G}]$	$2Ul_{U2S}$

We compare the proposed FedMeld with the following baseline algorithms.

- **HFL [10]**. In each global round, each serving satellite activates a subset of clients within its coverage area to perform  $E$  local iterations before aggregating the models from these clients. After  $K + \delta$  global rounds, the satellites transmit the aggregated models to a ground station for global aggregation. Upon re-establishing contact with the ground station, satellites receive the updated global model. In our experiments, two ground stations are used for global aggregation, with parameter sharing facilitated through ground optical fibers.
- **Parallel FL (PFL) [29]**. After satellites average the models from the devices within their coverage, they periodically exchange their parameters with neighboring satellites via ISLs, only once during each exchange period. In our experiments, the exchange period is set to  $K + \delta$  global rounds.
- **Ring Allreduce [16]**. Initially, the aggregated model of each satellite is divided into multiple chunks. Each satellite then sends a chunk to the next satellite while simultaneously receiving a chunk from the previous satellite. This iterative process continues until all data chunks are fully aggregated across all serving satellites, resulting in a synchronized model at each satellite. The parameter exchange period is also set to  $K + \delta$  global rounds. However, this scheme relies on tightly costly ISLs, which are not fully applied in many existing commercial SGINs.

### B. Communication Costs

Before evaluating the learning performance, Table II provides a comparison between FedMeld and three baseline algorithms with respect to learning type, model aggregation methods, and communication costs per global round. This analysis considers a scenario with  $M$  clusters and  $U$  participating clients. Here,  $\min$  refers to the optimal conditions for PFL and Ring Allreduce, where all satellites serving the clusters can establish ISLs with their neighbors. When these serving satellites cannot set up ISLs, the models of each area must be sent to the ground station. Therefore,  $\max$  denotes the worst-case scenario where any two satellites are not visible to each other. We can conclude that the proposed FedMeld is an infrastructure-independent framework with the lowest communication costs.

### C. Learning Performance

In this part, we evaluate the learning performance of various FL frameworks across two datasets under three distinct data distribution settings. Fig. 3 and Fig. 4 illustrate the learning performance of the FedMeld compared to three baseline schemes across different data distribution scenarios in each dataset.

- **IID clients**: Each user receives an equal number of samples randomly drawn from the entire dataset, with images assigned to users following an IID pattern.
- **IID clusters (with non-IID clients)**: Each cluster selects images in proportion to the number of users in that cluster, randomly drawing from all labels. Within each cluster, users are assigned an equal number of images, typically from an average of 3 labels.
- **Non-IID clusters (with non-IID clients)**: Clients within the same cluster receive images drawn from only 3 specific labels, and each client further selects images from 2 labels within the cluster's data.

From the experiment results, the following observations can be made: 1) The proposed FedMeld consistently achieves the highest model accuracy among all frameworks, demonstrating the superior performance of our approach. Compared to HFL, this decentralized FL scheme allows adjacent regions to mix parameters directly and update models more flexibly, avoiding the excessive time required for model aggregation at ground stations. The advantages of FedMeld over PFL and Ring Allreduce in terms of model accuracy stem from two key aspects: First, the careful design of mixing ratio and global round interval between adjacent regions. Second, FedMeld avoids reliance on ISLs that are not yet fully deployed across the entire constellation. 2) Ring Allreduce exhibits the fastest convergence speed. This is because, after the same number of global rounds, Ring Allreduce completes a full global average, whereas FedMeld and P-FedAvg perform local parameter exchanges between neighboring regions. 3) The model accuracy of P-FedAvg declines markedly as the non-IID degree of the data increases. 4) The accuracy of HFL is comparable to that of FedMeld. However, HFL always has the longest training time. This is because the aggregation frequency in HFL is determined by the interval between consecutive passes of all serving satellites over the ground stations.

Next, we will focus on the impact of key parameters on model accuracy and the time cost of model training. Given that the model accuracy under IID clients is quite similar across

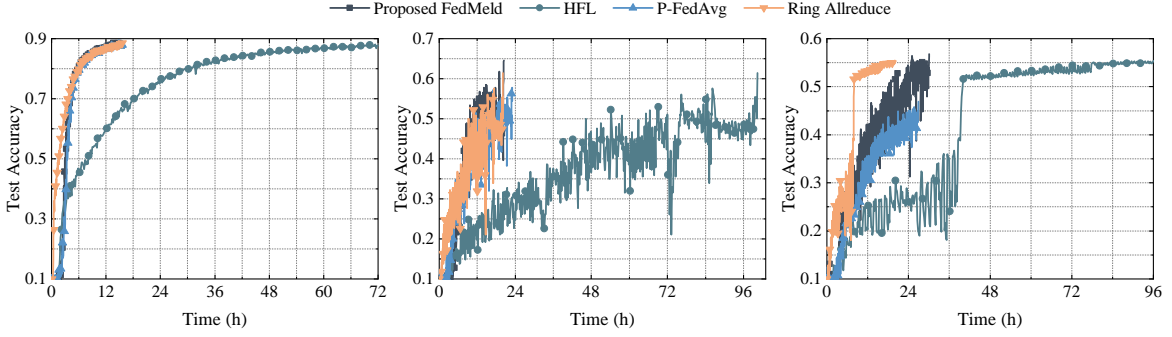


Fig. 3. Test accuracy versus time on CIFAR-10 with IID clients (left), IID clusters with non-IID clients (center), and non-IID clusters with non-IID clients (right).

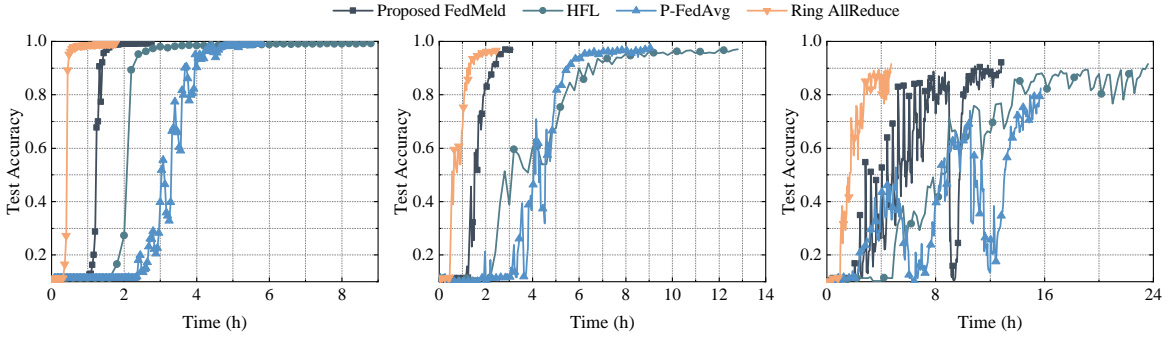


Fig. 4. Test accuracy versus time on MNIST in client IID (left), cluster IID with client non-IID (center), and cluster non-IID with client non-IID (right).

all frameworks, the subsequent discussion will focus solely on the non-IID cases under varying key parameters.

#### D. Effects of Satellite Number

We investigate the effect of the number of satellites on learning performance across different frameworks, as shown in Fig. 5 and Fig. 6. The number of satellites directly influences the session duration between space and ground, affecting learning performance by controlling  $K$ . As satellites become denser, the model accuracy of FedMeld initially improves and then declines in Fig. 5(a), while accuracy increases monotonically in other settings. Compared to other methods, FedMeld generally demonstrates superior model accuracy, except in the case of non-IID clusters in Fig. 6(a) with 88 satellites per orbit. Regarding training time, it shows a monotonically increasing trend due to the shorter serving time of each satellite. Additionally, dense satellite networks lead to more frequent handovers and increased launch costs. Thus, beyond the trade-off between model accuracy and training time, there is also a trade-off between learning performance and handover/engineering costs.

#### E. Effects of Latency Constraint

In Fig. 7 and Fig. 8, we analyze the impact of maximal tolerable delay  $T_{\max}$  on the performance of FedMeld. As the latency constraint becomes more relaxed, it allows more fresh parameter mixing when the serving satellite flies over the next cluster, i.e.,  $\delta^*$  is smaller. We observe that when

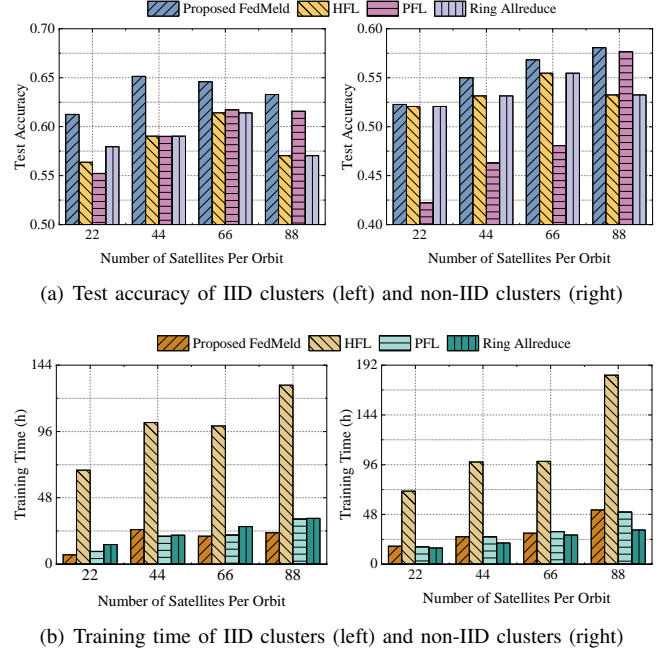
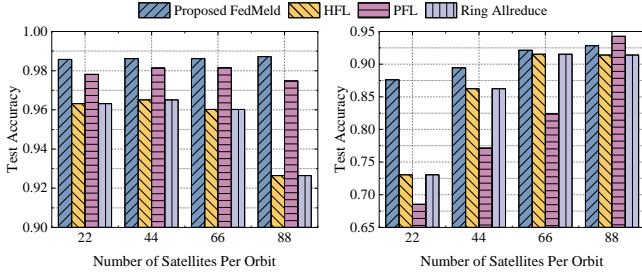
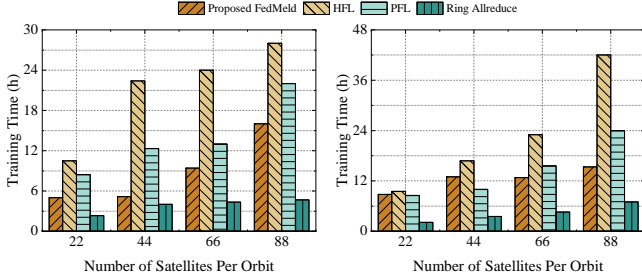


Fig. 5. Effect of satellite number on test accuracy and training time on CIFAR-10.

$T_{\max}$  increases, model accuracy improves while convergence speed slows. These observations confirm the effectiveness of the proof that the objective function  $f(\delta, \alpha)$  of  $\mathcal{P}1$  is monotonically increasing with respect to  $\delta$  in Lemma 4.

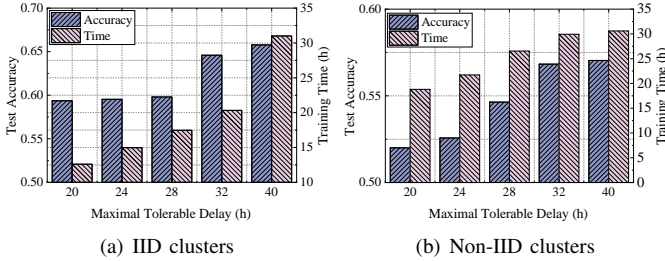


(a) Test accuracy of IID clusters (left) and non-IID clusters (right)



(b) Training time of IID clusters (left) and non-IID clusters (right)

Fig. 6. Effect of satellite number on test accuracy and training time on MNIST.



(a) IID clusters

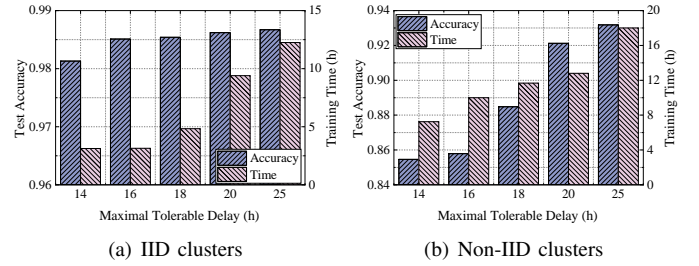
(b) Non-IID clusters

Fig. 7. Effect of maximal tolerable delay with different non-IID degrees on CIFAR-10.

## VI. CONCLUSION

In this paper, we propose the novel FedMeld framework for SGINs. By leveraging the predictable movement patterns and SCF capabilities of satellites, the infrastructure-free FedMeld enables parameter aggregation across different terrestrial regions without relying on ground stations or ISLs. Our findings indicate that the optimal global round interval of model mixing between adjacent areas is highly influenced by latency constraints and handover frequency, while the ideal mixing ratio of historical models from adjacent regions is determined by the degree of non-IID data distribution.

This work pioneers the concept of an infrastructure-free FL framework within the context of space-ground Fluid AI. The current FedMeld algorithm can be extended to more complex scenarios, such as implementing region-specific round intervals and adaptive mixing ratios. Practical challenges, such as balancing learning performance with handover and launch costs, merit further exploration. Additionally, investigating efficient inference strategies and model downloading mechanisms for SGINs represents a promising avenue for future research.



(a) IID clusters

(b) Non-IID clusters

Fig. 8. Effect of maximal tolerable delay with different non-IID degrees on MNIST.

## APPENDIX A PROOF OF THEOREM 1

From Assumption 3, the upper bound of  $\mathbb{E}\|\mathbf{g}_t - \bar{\mathbf{g}}_t\|^2$  follows that

$$\begin{aligned} & \mathbb{E}\|\mathbf{g}_t - \bar{\mathbf{g}}_t\|^2 \\ &= \left\| \sum_{i \in \mathcal{M}} \sum_{j \in \mathcal{N}_i} \frac{1}{MN_i} [\nabla F_j(\mathbf{w}_{t,j}^s, \mathbf{c}_{t,j}^s) - \nabla F_j(\mathbf{w}_{t,j})] \right\|^2 \\ &\leq \sum_{i \in \mathcal{M}} \sum_{j \in \mathcal{N}_i} \frac{\sigma_j^2}{(MN_i)^2}. \end{aligned} \quad (26)$$

Let  $\Delta_t = \mathbb{E}\|\bar{\mathbf{w}}_t - \mathbf{w}^*\|^2$ . By substituting (26) into (10), we have

$$\|\bar{\mathbf{w}}_{t+1} - \mathbf{w}^*\|^2 \leq (1 - \mu\eta_t) \Delta_t + \eta_t^2 B + 2Q_t, \quad (27)$$

where  $B = \sum_{i \in \mathcal{M}} \sum_{j \in \mathcal{N}_i} \frac{\sigma_j^2}{(MN_i)^2} + 6L\Gamma$  and  $Q_t = \mathbb{E} \sum_{i \in \mathcal{M}} \sum_{j \in \mathcal{N}_i} \frac{1}{MN_i} \|\bar{\mathbf{w}}_t - \mathbf{w}_{t,j}\|^2$ .

First, we discuss the case that  $A_{t+1} \neq 0$ . From (9), it is clear that when  $A_{t+1} \neq 0$ ,  $\bar{\mathbf{w}}_{t+1} = \bar{\mathbf{v}}_{t+1}$  holds, and we have

$$\Delta_{t+1} \leq (1 - \eta_t\mu) \Delta_t + \eta_t^2 B + 2Q_t. \quad (28)$$

Thus, we only need to verify  $\Delta_{t+1} \leq (1 - \eta_t\mu) \Delta_t + \eta_t^2 B$ , and then (28) always holds.

Choose a diminishing stepsize learning rate  $\eta_t = \frac{\beta}{t+\gamma}$  for some  $\mu\beta > 1$  and  $\gamma > 0$  such that  $\eta_1 \leq \min\left\{\frac{1}{\mu}, \frac{1}{4L}\right\} = \frac{1}{4L}$  and  $\eta_t \leq 2\eta_{t+E}$ . By setting  $v = \max\left\{\frac{\beta^2 B}{\beta\mu-1}, (\gamma+1)\Delta_1\right\}$ , then we will prove  $\Delta_t \leq \left(\frac{1}{1-\alpha} - \alpha + \frac{1}{2}\right) \frac{v}{t+\gamma}$  for  $A_{t+1} \neq 0$ . Assume that this conclusion holds for some  $t$ , then we have

$$\begin{aligned} \Delta_{t+1} &\leq (1 - \eta_t\mu) \Delta_t + \eta_t^2 B \\ &\leq \left(1 - \frac{\mu\beta}{t+\gamma}\right) \left(\frac{1}{1-\alpha} - \alpha + \frac{1}{2}\right) \frac{v}{t+\gamma} + \frac{B\beta^2}{(t+\gamma)^2} \\ &= \frac{t+\gamma-1}{(t+\gamma)^2} \left(\frac{1}{1-\alpha} - \alpha + \frac{1}{2}\right) v \\ &+ \left[ \frac{B\beta^2}{(t+\gamma)^2} - \frac{\mu\beta-1}{(t+\gamma)^2} \left(\frac{1}{1-\alpha} - \alpha + \frac{1}{2}\right) v \right] \\ &\leq \left(\frac{1}{1-\alpha} - \alpha + \frac{1}{2}\right) \frac{t+\gamma-1}{(t+\gamma)^2} v \end{aligned} \quad (29)$$

$$\leq \left( \frac{1}{1-\alpha} - \alpha + \frac{1}{2} \right) \frac{1}{t+\gamma+1} v,$$

where (29) follows from  $B\beta^2 \leq (\mu\beta - 1)v$  and  $\frac{1}{1-\alpha} - \alpha + \frac{1}{2} > 1$ .

Then, we discuss the case that  $A_{t+1} = 1$ . When  $A_{t+1} = 1$ , we have  $\bar{\mathbf{w}}_{t+1} = (1-\alpha)\bar{\mathbf{v}}_{t+1} + \alpha\bar{\mathbf{w}}_{t+1-\delta E}$ . Then, the lower bounded of  $\mathbb{E}\|\bar{\mathbf{v}}_{t+1} - \mathbf{w}^*\|^2$  can be obtained as follows.

$$\begin{aligned} & \mathbb{E}\|\bar{\mathbf{v}}_{t+1} - \mathbf{w}^*\|^2 \\ &= \mathbb{E}\left\| \frac{\bar{\mathbf{w}}_{t+1} - \alpha\bar{\mathbf{w}}_{t+1-\delta E}}{1-\alpha} - \mathbf{w}^* \right\|^2 \\ &= \mathbb{E}\left\| \frac{1}{1-\alpha} (\bar{\mathbf{w}}_{t+1} - \mathbf{w}^*) - \frac{\alpha}{1-\alpha} (\bar{\mathbf{w}}_{t+1-\delta E} - \mathbf{w}^*) \right\|^2 \\ &= \frac{1}{(1-\alpha)^2} \|\bar{\mathbf{w}}_{t+1} - \mathbf{w}^*\|^2 + \frac{\alpha^2}{(1-\alpha)^2} \|\bar{\mathbf{w}}_{t+1-\delta E} - \mathbf{w}^*\|^2 \\ &\quad - \frac{2\alpha}{(1-\alpha)^2} \langle \bar{\mathbf{w}}_{t+1} - \mathbf{w}^*, \bar{\mathbf{w}}_{t+1-\delta E} - \mathbf{w}^* \rangle \\ &\geq \frac{1}{1-\alpha} \|\bar{\mathbf{w}}_{t+1} - \mathbf{w}^*\|^2 - \frac{\alpha}{1-\alpha} \|\bar{\mathbf{w}}_{t+1-\delta E} - \mathbf{w}^*\|^2, \quad (30) \end{aligned}$$

The last inequality comes from Cauchy-Schwarz Inequality and Young's inequality:

$$\begin{aligned} & \langle \bar{\mathbf{w}}_{t+1} - \mathbf{w}^*, \bar{\mathbf{w}}_{t+1-\delta E} - \mathbf{w}^* \rangle \\ &\leq \|\bar{\mathbf{w}}_{t+1} - \mathbf{w}^*\| \|\bar{\mathbf{w}}_{t+1-\delta E} - \mathbf{w}^*\| \\ &\leq \frac{1}{2} \left( \|\bar{\mathbf{w}}_{t+1} - \mathbf{w}^*\|^2 + \|\bar{\mathbf{w}}_{t+1-\delta E} - \mathbf{w}^*\|^2 \right). \end{aligned}$$

By substituting (30) into (27), we have

$$\Delta_{t+1} \leq (1-\alpha) \left[ (1-\eta_t\mu) \Delta_t + \eta_t^2 B \right] + \alpha \Delta_{t+1-\delta E} + 2Q_t, \quad (31)$$

Similarly, we only need to verify  $\Delta_{t+1} \leq (1-\alpha) \left[ (1-\eta_t\mu) \Delta_t + \eta_t^2 B \right] + \alpha \Delta_{t+1-\delta E}$ , and then (31) always holds. We also prove  $\Delta_t \leq \left( \frac{1}{1-\alpha} - \alpha + \frac{1}{2} \right) \frac{v}{t+\gamma}$  by induction. Assume that this conclusion holds for some  $t$ , then we have

$$\begin{aligned} \Delta_{t+1} &\leq (1-\alpha) (1-\eta_t\mu) \Delta_t + (1-\alpha) \eta_t^2 B + \alpha \Delta_{t+1-\delta E} \\ &\leq \left( 1 - \frac{\mu\beta}{t+\gamma} \right) \frac{(2\alpha^2 - 3\alpha + 3)v}{2(t+\gamma)} + \frac{(1-\alpha)B\beta^2}{(t+\gamma)^2} \\ &\quad + \frac{\alpha(2\alpha^2 - 3\alpha + 3)v}{2(1-\alpha)(t+1-\delta E + \gamma)} \\ &= \frac{(2\alpha^2 - 3\alpha + 3)(t+\gamma-1)v}{2(t+\gamma)^2} + \frac{\alpha(2\alpha^2 - 3\alpha + 3)v}{2(1-\alpha)(t+1-\delta E + \gamma)} \\ &\quad - \frac{(2\alpha^2 - \alpha + 1)(\mu\beta - 1)v}{2(t+\gamma)^2} \\ &\quad + (1-\alpha) \left[ \frac{B\beta^2}{(t+\gamma)^2} - \frac{\mu\beta - 1}{(t+\gamma)^2} v \right] \\ &\leq \frac{(2\alpha^2 - 3\alpha + 3)(t+\gamma-1)v}{2(t+\gamma)^2} + \frac{\alpha(2\alpha^2 - 3\alpha + 3)v}{2(1-\alpha)(t+1-\delta E + \gamma)} \\ &\quad - \frac{(2\alpha^2 - \alpha + 1)(\mu\beta - 1)v}{2(t+\gamma)^2} \\ &\leq \left( \frac{1}{1-\alpha} - \alpha + \frac{1}{2} \right) \frac{v}{t+\gamma+1}. \quad (32) \end{aligned}$$

When  $\delta E \leq \frac{m(\alpha)(t+\gamma+1)^2}{(t+\gamma)^2 + m(\alpha)(t+\gamma+1)}$ , the last inequality of (32) holds.

By setting  $\beta = \frac{5}{\mu}$  and  $\gamma = \max \left\{ \frac{8L}{\mu}, E \right\} - 1$ , then  $\eta_t$  satisfies  $\eta_t \leq 2\eta_{t+E}$  for any step  $t$ . Then, we have

$$\begin{aligned} v &= \max \left\{ \frac{\beta^2 B}{\beta\mu - 1}, (\gamma+1)\Delta_1 \right\} \leq \frac{\beta^2 B}{\beta\mu - 1} + (\gamma+1)\Delta_1 \\ &\leq \frac{25B}{4\mu^2} + (\gamma+1)\Delta_1. \end{aligned}$$

According to Assumption 1, the convergence upper bound can be given by

$$\begin{aligned} \mathbb{E}[F(\bar{\mathbf{w}}_t)] - F(\mathbf{w}^*) &\leq \frac{L}{2} \Delta_t \\ &\leq \frac{L}{2} \left[ \left( \frac{1}{1-\alpha} - \alpha + \frac{1}{2} \right) \frac{v}{t+\gamma} + 2Q_{t-1} \right] \\ &\leq \left( \frac{1}{1-\alpha} - \alpha + \frac{1}{2} \right) \frac{L}{\mu(t+\gamma)} \left[ \frac{25B}{8\mu} + \frac{\mu(\gamma+1)}{2} \Delta_1 \right] + LQ_{t-1}. \quad (33) \end{aligned}$$

This completes the proof.

## APPENDIX B PROOF OF LEMMA 2

We introduce an auxiliary variable  $\tilde{t}$ . When  $t \notin \mathcal{I}_E$ , then  $\tilde{t} = \lfloor t/E \rfloor E$ . When  $t \in \mathcal{I}_E$ ,  $\tilde{t} = t - E$  holds. Then, the update rule of local model can be written as

$$\mathbf{w}_{t,j} = \begin{cases} \mathbf{w}_{\tilde{t},j} - \sum_{s=\tilde{t}}^{t-1} \eta_s \mathbf{g}_{s,j}, & \text{if } t \notin \mathcal{I}_E, \\ \frac{1-\alpha A_t}{N_i} \sum_{j \in \mathcal{N}_i} \left( \mathbf{w}_{\tilde{t},j} - \sum_{s=\tilde{t}}^{t-1} \eta_s \mathbf{g}_{s,j} \right) + \alpha A_t \bar{\mathbf{w}}_{t-\delta E, i-1}, & \text{if } t \in \mathcal{I}_E, \end{cases} \quad (34)$$

where  $\mathbf{g}_{s,j} = \nabla F_j(\mathbf{w}_{s,j}, \mathcal{S}_{s,j})$  for notational brevity. The virtual global model can be written as

$$\begin{aligned} \bar{\mathbf{w}}_t &= (1-\alpha A_t) \bar{\mathbf{v}}_t + \alpha A_t \bar{\mathbf{w}}_{t-\delta E} \\ &= \frac{1}{M} \sum_{i \in \mathcal{M}} \left[ (1-\alpha A_t) \left( \bar{\mathbf{w}}_{\tilde{t},i} - \sum_{s=\tilde{t}}^{t-1} \eta_s \mathbf{g}_{s,i} \right) + \alpha A_t \bar{\mathbf{w}}_{t-\delta E, i-1} \right]. \quad (35) \end{aligned}$$

First, we discuss the upper bound of  $Q_t$  when  $t \in \mathcal{I}_E$ , and we have

$$\begin{aligned} \mathbb{E}Q_t &= \sum_{i \in \mathcal{M}} \sum_{j \in \mathcal{N}_i} \frac{1}{MN_i} \mathbb{E} \|\mathbf{w}_{t,j} - \bar{\mathbf{w}}_t\|^2 \\ &= \sum_{i \in \mathcal{M}} \sum_{j \in \mathcal{N}_i} \frac{1}{MN_i} \mathbb{E} \left\| (1-\alpha A_t) (\mathbf{w}_{\tilde{t},j} - \bar{\mathbf{w}}_{\tilde{t}}) \right. \\ &\quad \left. + \alpha A_t \left( \bar{\mathbf{w}}_{t-\delta E, i-1} - \frac{1}{M} \sum_{i \in \mathcal{M}} \bar{\mathbf{w}}_{t-\delta E, i-1} \right) \right. \\ &\quad \left. - (1-\alpha A_t) \left( \sum_{s=\tilde{t}}^{t-1} \eta_s \mathbf{g}_{s,j} - \frac{1}{M} \sum_{i \in \mathcal{M}} \sum_{s=\tilde{t}}^{t-1} \eta_s \mathbf{g}_{s,i} \right) \right\|^2 \\ &\leq (1+b) \sum_{i \in \mathcal{M}} \sum_{j \in \mathcal{N}_i} \frac{1}{MN_i} \mathbb{E} \left\| (1-\alpha A_t) (\mathbf{w}_{\tilde{t},j} - \bar{\mathbf{w}}_{\tilde{t}}) \right. \\ &\quad \left. + \alpha A_t (\bar{\mathbf{w}}_{t-\delta E, i-1} - \bar{\mathbf{w}}_{t-\delta E}) \right\|^2 \end{aligned}$$

$$\begin{aligned}
& + \left(1 + \frac{1}{b}\right) \sum_{i \in \mathcal{M}} \sum_{j \in \mathcal{N}_i} \frac{1}{MN_i} \mathbb{E} \|(1 - \alpha A_t) \\
& \cdot \left( \sum_{s=\bar{t}}^{t-1} \eta_s \mathbf{g}_{s,j} - \frac{1}{M} \sum_{i \in \mathcal{M}} \sum_{s=\bar{t}}^{t-1} \eta_s \mathbf{g}_{s,i} \right) \|^2 \quad (36) \\
& \leq (1+b)(1 - \alpha A_t)^2 \sum_{i \in \mathcal{M}} \sum_{j \in \mathcal{N}_i} \frac{1}{MN_i} \mathbb{E} \|\mathbf{w}_{\bar{t},j} - \bar{\mathbf{w}}_{\bar{t}}\|^2 \\
& + (1+b)(\alpha A_t)^2 \sum_{i \in \mathcal{M}} \sum_{j \in \mathcal{N}_i} \frac{1}{MN_i} \mathbb{E} \|\bar{\mathbf{w}}_{t-\delta E, i-1} - \bar{\mathbf{w}}_{t-\delta E}\|^2 \\
& + \left(1 + \frac{1}{b}\right) (1 - \alpha A_t)^2 \sum_{i \in \mathcal{M}} \sum_{j \in \mathcal{N}_i} \frac{1}{MN_i} \\
& \cdot \mathbb{E} \left\| \sum_{s=\bar{t}}^{t-1} \eta_s \mathbf{g}_{s,j} - \frac{1}{M} \sum_{i \in \mathcal{M}} \sum_{s=\bar{t}}^{t-1} \eta_s \mathbf{g}_{s,i} \right\|^2 \quad (37) \\
& \leq (1+b)(1 - \alpha A_t)^2 Q_{\bar{t}} + (1+b)(\alpha A_t)^2 Q_{t-\delta E} \\
& + 4 \left(1 + \frac{1}{b}\right) (1 - \alpha A_t)^2 (E-1)^2 G^2 \eta_{\bar{t}}^2,
\end{aligned}$$

where we use Jensen inequality in (36). That is, for any  $X_1, X_2 \in \mathbb{R}^d$ ,  $\|X_1 + X_2\|^2 \leq (1+b)\|X_1\|^2 + \left(1 + \frac{1}{b}\right)\|X_2\|^2$ , where  $b$  can be any positive real number. In (37), the first two terms come from the convexity of  $\|\cdot\|^2$ , and the expectation in the last term can be calculated by

$$\begin{aligned}
\mathbb{E} \left\| \sum_{s=\bar{t}}^{t-1} \eta_s \mathbf{g}_{s,j} - \frac{1}{M} \sum_{i \in \mathcal{M}} \sum_{s=\bar{t}}^{t-1} \eta_s \mathbf{g}_{s,i} \right\|^2 & \leq \mathbb{E} \left\| \sum_{s=\bar{t}}^{t-1} \eta_s \mathbf{g}_{s,j} \right\|^2 \\
& \leq \mathbb{E} \left\| \sum_{s=\bar{t}}^{t-1} \eta_t \mathbf{g}_{s,j} \right\|^2 \leq 4\eta_t^2 (E-1)^2 G^2,
\end{aligned}$$

where the first inequality comes from  $\mathbb{E}\|X - \mathbb{E}X\|^2 \leq \mathbb{E}\|X\|^2$ .

When  $t \notin \mathcal{I}_E$ , we have

$$\begin{aligned}
\mathbb{E}Q_t & = \sum_{i \in \mathcal{M}} \sum_{j \in \mathcal{N}_i} \frac{1}{MN_i} \mathbb{E} \|\mathbf{w}_{t,j} - \bar{\mathbf{w}}_t\|^2 \\
& = \sum_{i \in \mathcal{M}} \sum_{j \in \mathcal{N}_i} \frac{1}{MN_i} \mathbb{E} \left\| (\mathbf{w}_{\bar{t},j} - \bar{\mathbf{w}}_{\bar{t}}) \right. \\
& \left. - \left( \sum_{s=\bar{t}}^{t-1} \eta_s \mathbf{g}_{s,j} - \frac{1}{M} \sum_{i \in \mathcal{M}} \sum_{s=\bar{t}}^{t-1} \eta_s \mathbf{g}_{s,i} \right) \right\|^2 \\
& \leq (1+b) \sum_{i \in \mathcal{M}} \sum_{j \in \mathcal{N}_i} \frac{1}{MN_i} \mathbb{E} \|\mathbf{w}_{\bar{t},j} - \bar{\mathbf{w}}_{\bar{t}}\|^2 \\
& + \left(1 + \frac{1}{b}\right) \sum_{i \in \mathcal{M}} \sum_{j \in \mathcal{N}_i} \frac{1}{MN_i} \\
& \cdot \mathbb{E} \left\| \sum_{s=\bar{t}}^{t-1} \eta_s \mathbf{g}_{s,j} - \frac{1}{M} \sum_{i \in \mathcal{M}} \sum_{s=\bar{t}}^{t-1} \eta_s \mathbf{g}_{s,i} \right\|^2 \\
& \leq (1+b)Q_{\bar{t}} + 4 \left(1 + \frac{1}{b}\right) E^2 G^2 \eta_{\bar{t}}^2.
\end{aligned}$$

This completes the proof.

## APPENDIX C PROOF OF THEOREM 2

First, we define the following variables  $C_1 - C_5$  for notational brevity. That is,  $C_1 = (1+b)(1-\alpha)^2$ ,  $C_2 = (1+b)\alpha^2$ ,  $C_3 = 4\left(1 + \frac{1}{b}\right)(1-\alpha)^2(E-1)^2G^2$ ,  $C_4 = (1+b)$ , and  $C_5 = 4\left(1 + \frac{1}{b}\right)(E-1)^2G^2$ . When  $R-1$  is the step of different area mixing models, i.e.,  $A_{R-1} = 1$ , we have the following set of inequalities from step  $R-1 - (K+\delta)E + E$  to  $R-1$  based on (12).

$$\begin{cases} Q_{R-1} \leq C_1 Q_{R-1-E} + C_2 Q_{R-1-\delta E} + C_3 \eta_{R-1}^2, \\ Q_{R-1-E} \leq C_4 Q_{R-1-2E} + C_5 \eta_{R-1-E}^2, \\ \dots \\ Q_{R-1-(K+\delta)E+E} \leq C_4 Q_{R-1-(K+\delta)E} + C_5 \eta_{R-1-(K+\delta)E+E}^2. \end{cases}$$

Based on the recurrence relation, we have

$$Q_{R-1} \leq \kappa_1 Q_{R-1-(K+\delta)E} + \kappa_2 \eta_{R-1-(K+\delta)E+E}^2, \quad (38)$$

where  $\kappa_1 = C_1(C_4)^{K+\delta-1} + C_2(C_4)^R = (1+b)^{K+\delta}(1-\alpha)^2 + (1+b)^{K+1}\alpha^2$  and  $\kappa_2 = C_1 C_5 \sum_{l=1}^{K+\delta-1} (C_4)^{l-1} + C_2 C_5 \sum_{l=\delta}^{K+\delta-1} (C_4)^{l-\delta} + C_3 = 4\left(1 + \frac{1}{b}\right)(E-1)^2G^2 \left[ \frac{(1+b)^{K+\delta}(1-\alpha)^2 + (1+b)^{K+1}\alpha^2}{b} + (1-\alpha)^2 \right]$ .

Assume that  $R-1 = q(K+\delta)E$ , where  $q$  denotes the total model mixing times from  $t=0$  to  $R-1$ . With the similar form of (38), we have the following inequalities of  $Q_t$  when  $A_t = 1$ .

$$\begin{cases} Q_{R-1} \leq \kappa_1 Q_{R-1-(K+\delta)E} + \kappa_2 \eta_{R-1-(K+\delta)E+E}^2, \\ Q_{R-1-(K+\delta)E} \leq \kappa_1 Q_{R-1-2(K+\delta)E} + \kappa_2 \eta_{R-1-2(K+\delta)E+E}^2, \\ \dots \\ Q_{R-1-(q-1)(K+\delta)E} \leq \kappa_1 Q_{R-1-q(K+\delta)E} + \kappa_2 \eta_{R-1-q(K+\delta)E+E}^2, \end{cases}$$

where the last inequality can also be represented by  $Q_E \leq \kappa_1 Q_0 + \kappa_2 \eta_E^2$ . According to the recurrence relationship,  $Q_{R-1}$  can be upper bounded by

$$\begin{aligned}
Q_{R-1} & \leq \kappa_1^q Q_0 + \kappa_2 \sum_{l=0}^{q-1} \kappa_1^l \eta_{R-1-(l+1)(K+\delta)E}^2 \\
& = \kappa_2 \sum_{l=0}^{q-1} \kappa_1^l \eta_{R-1-(l+1)(K+\delta)E}^2 \\
& \leq \eta_E^2 \kappa_2 \sum_{l=0}^{q-1} \kappa_1^l \leq \eta_E^2 \frac{\kappa_2}{1 - \kappa_1},
\end{aligned}$$

where the first equality follows from  $Q_0 = 0$  due to initialization. This completes the proof.

## APPENDIX D PROOF OF THEOREM 3

According to Lemma 3,  $\mathbb{E}_{\mathcal{U}_t} \|\bar{\mathbf{z}}_t - \mathbf{w}^*\|^2$  has the following upper bound,

$$\begin{aligned}
\mathbb{E}_{\mathcal{U}_t} \|\bar{\mathbf{z}}_t - \mathbf{w}^*\|^2 & = \mathbb{E}_{\mathcal{U}_t} \|\bar{\mathbf{z}}_t - \bar{\mathbf{w}}_t + \bar{\mathbf{w}}_t - \mathbf{w}^*\|^2 \\
& = \mathbb{E}_{\mathcal{U}_t} \|\bar{\mathbf{z}}_t - \bar{\mathbf{w}}_t\|^2 + \|\bar{\mathbf{w}}_t - \mathbf{w}^*\|^2 + 2\mathbb{E}_{\mathcal{U}_t} \langle \bar{\mathbf{z}}_t - \bar{\mathbf{w}}_t, \bar{\mathbf{w}}_t - \mathbf{w}^* \rangle \quad (39)
\end{aligned}$$

$$\begin{aligned}
&\leq \frac{1}{M^2} \sum_{i \in \mathcal{M}} \frac{N_i - U_i}{U_i N_i (N_i - 1)} \sum_{j \in \mathcal{N}_i} \|\mathbf{w}_{t,j} - \bar{\mathbf{w}}_t\|^2 + \|\bar{\mathbf{w}}_t - \mathbf{w}^*\|^2 \\
&\leq \max_{i \in \mathcal{M}} \left\{ \frac{N_i - U_i}{M U_i (N_i - 1)} \right\} \sum_{i \in \mathcal{M}} \sum_{j \in \mathcal{N}_i} \frac{1}{M N_i} \|\mathbf{w}_{t,j} - \bar{\mathbf{w}}_t\|^2 \\
&+ \|\bar{\mathbf{w}}_t - \mathbf{w}^*\|^2 \\
&= \max_{i \in \mathcal{M}} \left\{ \frac{N_i - U_i}{M U_i (N_i - 1)} \right\} Q_t + \Delta_t,
\end{aligned}$$

where the last term in (39) is eliminated in the next line due to the unbiasedness of  $\bar{\mathbf{z}}_t$ . Similar to (33), we have

$$\begin{aligned}
\mathbb{E}[F(\bar{\mathbf{z}}_t)] - F(\mathbf{w}^*) &\leq \frac{L}{2} \mathbb{E}_{\mathcal{U}_t} \|\bar{\mathbf{z}}_t - \mathbf{w}^*\|^2 \\
&\leq \frac{L}{2} \left[ \max_{i \in \mathcal{M}} \left\{ \frac{N_i - U_i}{M U_i (N_i - 1)} \right\} Q_t \right. \\
&\quad \left. + \left( \frac{1}{1 - \alpha} - \alpha + \frac{1}{2} \right) \frac{v}{t + \gamma} + 2Q_{t-1} \right].
\end{aligned}$$

When  $t = R$  and  $A_{R-1} = 1$ ,  $Q_R$  can be obtained by (13) where  $\tilde{t} = R - 1$ . This completes the proof.

## REFERENCES

- [1] K. B. Letaief, W. Chen, Y. Shi, J. Zhang, and Y.-J. A. Zhang, "The roadmap to 6G: AI empowered wireless networks," *IEEE Commun. Mag.*, vol. 57, no. 8, pp. 84–90, Aug. 2019.
- [2] G. Qu, Q. Chen, W. Wei, Z. Lin, X. Chen, and K. Huang, "Mobile edge intelligence for large language models: A contemporary survey," *arXiv preprint arXiv:2407.18921*, 2024.
- [3] M. Sheng, D. Zhou, W. Bai, J. Liu, H. Li, Y. Shi, and J. Li, "Coverage enhancement for 6G satellite-terrestrial integrated networks: performance metrics, constellation configuration and resource allocation," *Sci. China Inform. Sci.*, vol. 66, no. 3, p. 130303, Mar. 2023.
- [4] SpaceX, "SpaceX: We've launched 32,000 linux computers into space for starlink internet," Jun. 2020. [Online]. Available: <https://www.zdnet.com/article/>
- [5] Q. Chen, Z. Wang, X. Chen, J. Wen, D. Zhou, S. Ji, M. Sheng, and K. Huang, "Space-ground fluid AI for 6G edge intelligence," *arXiv preprint arXiv:2411.15845*, 2024.
- [6] Q. Chen, Z. Guo, W. Meng, S. Han, C. Li, and T. Q. S. Quek, "A survey on resource management in joint communication and computing-embedded SAGIN," *IEEE Commun. Surveys Tuts.*, Early access, Jul. 01, 2024.
- [7] B. McMahan, E. Moore, D. Ramage, S. Hampson, and B. A. y Arcas, "Communication-efficient learning of deep networks from decentralized data," in *Proc. Artificial intelligence and statistics*, Ft. Lauderdale, FL, USA, Apr. 2017, pp. 1273–1282.
- [8] Z. Wang, K. Huang, and Y. C. Eldar, "Spectrum breathing: Protecting over-the-air federated learning against interference," *IEEE Trans. Wireless Commun.*, vol. 23, no. 8, pp. 10 058–10 071, Aug. 2024.
- [9] H. Yang, W. Liu, H. Li, and J. Li, "Maximum flow routing strategy for space information network with service function constraints," *IEEE Trans. Wireless Commun.*, vol. 21, no. 5, pp. 2909–2923, May 2022.
- [10] B. Matthiesen, N. Razmi, I. Leyva-Mayorga, A. Dekorsy, and P. Popovski, "Federated learning in satellite constellations," *IEEE Network*, vol. 38, no. 2, pp. 232–239, Mar. 2024.
- [11] Z. Lin, Z. Chen, Z. Fang, X. Chen, X. Wang, and Y. Gao, "FedSN: A federated learning framework over heterogeneous LEO satellite networks," *IEEE Trans. Mobile Comput.*, Early access, Oct. 15, 2024.
- [12] Y. Huang, X. Li, M. Zhao, H. Li, and M. Peng, "Asynchronous federated learning via over-the-air computation in LEO satellite networks," *IEEE Trans. Wireless Commun.*, Early access, Nov. 06, 2024.
- [13] J. So, K. Hsieh, B. Arzani, S. Noghabi, S. Avestimehr, and R. Chandra, "FedSpace: An efficient federated learning framework at satellites and ground stations," *arXiv preprint arXiv:2202.01267*, 2022.
- [14] N. Razmi, B. Matthiesen, A. Dekorsy, and P. Popovski, "Ground-assisted federated learning in LEO satellite constellations," *IEEE Wireless Commun. Lett.*, vol. 11, no. 4, pp. 717–721, Apr. 2022.
- [15] D.-J. Han, S. Hosseinalipour, D. J. Love, M. Chiang, and C. G. Brinton, "Cooperative federated learning over ground-to-satellite integrated networks: Joint local computation and data offloading," *IEEE J. Sel. Areas Commun.*, vol. 42, no. 5, pp. 1080–1096, May 2024.
- [16] Q. Fang, Z. Zhai, S. Yu, Q. Wu, X. Gong, and X. Chen, "Olive branch learning: A topology-aware federated learning framework for space-air-ground integrated network," *IEEE Trans. Wireless Commun.*, vol. 22, no. 7, pp. 4534–4551, Jul. 2023.
- [17] X. Linsel, "Optical comms' ecosystem setting up for the technological breakthrough," Optical satellite communications, 2023.
- [18] R. S. Frederiksen, T. G. Mulvad, I. Leyva-Mayorga, T. K. Madsen, and F. Chiariotti, "End-to-end delivery in LEO mega-constellations and the reordering problem," *arXiv preprint arXiv:2405.07627*, 2024.
- [19] S. Dou, S. Zhang, and K. L. Yeung, "Achieving predictable and scalable load balancing performance in LEO mega-constellations," in *Proc. ICC 2024 - IEEE International Conference on Communications*, Denver, USA, Jun. 2024, pp. 3146–3151.
- [20] M. Chen, H. V. Poor, W. Saad, and S. Cui, "Performance optimization of federated learning over mobile wireless networks," in *Proc. 2020 IEEE 21st International Workshop on Signal Processing Advances in Wireless Communications (SPAWC)*, Atlanta, USA, May 2020, pp. 1–5.
- [21] C. Feng, H. H. Yang, D. Hu, Z. Zhao, T. Q. S. Quek, and G. Min, "Mobility-aware cluster federated learning in hierarchical wireless networks," *IEEE Trans. Wireless Commun.*, vol. 21, no. 10, pp. 8441–8458, Oct. 2022.
- [22] Y. Peng, X. Tang, Y. Zhou, Y. Hou, J. Li, Y. Qi, L. Liu, and H. Lin, "How to tame mobility in federated learning over mobile networks?" *IEEE Trans. Wireless Commun.*, vol. 22, no. 12, pp. 9640–9657, Dec. 2023.
- [23] T. Chen, J. Yan, Y. Sun, S. Zhou, D. Gündüz, and Z. Niu, "Mobility accelerates learning: Convergence analysis on hierarchical federated learning in vehicular networks," *arXiv preprint arXiv:2401.09656*, 2024.
- [24] Q. Chen, L. Yang, Y. Zhao, Y. Wang, H. Zhou, and X. Chen, "Shortest path in LEO satellite constellation networks: An explicit analytic approach," *IEEE J. Sel. Areas Commun.*, vol. 42, no. 5, pp. 1175–1187, May 2024.
- [25] F. Wang, D. Jiang, Z. Wang, J. Chen, and T. Q. S. Quek, "Seamless handover in LEO based non-terrestrial networks: Service continuity and optimization," *IEEE Trans. Commun.*, vol. 71, no. 2, pp. 1008–1023, Feb. 2023.
- [26] X. Li, K. Huang, W. Yang, S. Wang, and Z. Zhang, "On the convergence of FedAvg on non-IID data," in *Proc. Int. Conf. Learn. Represent.*, Apr.-May 2020. [Online]. Available: <https://arxiv.org/abs/1907.02189>
- [27] Z. Jia, M. Sheng, J. Li, D. Zhou, and Z. Han, "Joint HAP access and LEO satellite backhaul in 6G: Matching game-based approaches," *IEEE J. Sel. Areas Commun.*, vol. 39, no. 4, pp. 1147–1159, Apr. 2021.
- [28] A. Al-Hourani, "Session duration between handovers in dense LEO satellite networks," *IEEE Wireless Commun. Lett.*, vol. 10, no. 12, pp. 2810–2814, Oct. 2021.
- [29] X. Liu, Z. Yan, Y. Zhou, D. Wu, X. Chen, and J. H. Wang, "Optimizing parameter mixing under constrained communications in parallel federated learning," *IEEE/ACM Trans. Netw.*, vol. 31, no. 6, pp. 2640–2652, Dec. 2023.
- [30] A. Krizhevsky, G. Hinton *et al.*, "Learning multiple layers of features from tiny images," University of Toronto, Toronto, ON, Canada, Tech. Rep., 2009.
- [31] Y. Lecun, L. Bottou, Y. Bengio, and P. Haffner, "Gradient-based learning applied to document recognition," *Proc. IEEE*, vol. 86, no. 11, pp. 2278–2324, Nov. 1998.
- [32] K. He, X. Zhang, S. Ren, and J. Sun, "Deep residual learning for image recognition," in *Proc. 2016 IEEE Conference on Computer Vision and Pattern Recognition (CVPR)*, Las Vegas, USA, Jun. 2016, pp. 770–778.
- [33] Z. Lin, G. Zhu, Y. Deng, X. Chen, Y. Gao, K. Huang, and Y. Fang, "Efficient parallel split learning over resource-constrained wireless edge networks," *IEEE Trans. Mobile Comput.*, vol. 23, no. 10, pp. 9224–9239, Oct. 2024.
- [34] Q. Chen, W. Meng, T. Q. S. Quek, and S. Chen, "Multi-tier hybrid offloading for computation-aware IoT applications in civil aircraft-augmented sagin," *IEEE J. Sel. Areas Commun.*, vol. 41, no. 2, pp. 399–417, Feb. 2023.